SAND 2013-2764P

2.1.2.1 Hydrodynamics FY12 Q4 Report

SNL-EFDC Model Application to Scotlandville Bend, Mississippi River

Janet Barco*, Jesse Roberts*, Erick Johnson*, and Scott James†

*Sandia National Laboratories

†E^x^ponent Inc.

December 2012

Sandia National Laboratories is a multi-program laboratory managed and operated by Sandia Corporation, a wholly owned subsidiary of Lockheed Martin Corporation, for the U.S. Department of Energy's National Nuclear Security Administration under contract DE-AC04-94AL85000.

Table of Contents

Table of Figures

Table of Tables

Summary and Key Accomplishments

This work presents the modeling results for an MHK field site on the Mississippi River at Scotlandville Bend, Baton Rouge, Louisiana (Figure 1). Potential changes to the physical environment imposed by operation of MHK turbine arrays were evaluated using the modeling platform SNL-EFDC. Three MHK-turbine array scenarios (ranging from pilot- to commercial-scale) were defined by Free Flow Power (FFP) to support their plans for future deployments. Model results with and without an MHK array for the three scenarios were compared to understand how the size of an MHK array might alter the Scotlandville Bend hydrodynamic environment. The contribution of power generation from individual turbines on a given pile and for the entire array was analyzed. A preliminary sediment shear stress and bed erosion model are also presented. However, the impacts of sediment transport will be the focus of future studies. These simulations and scenario analyses can assist cost-effective planning before proceeding to detailed siting, engineering designs, and device deployment.

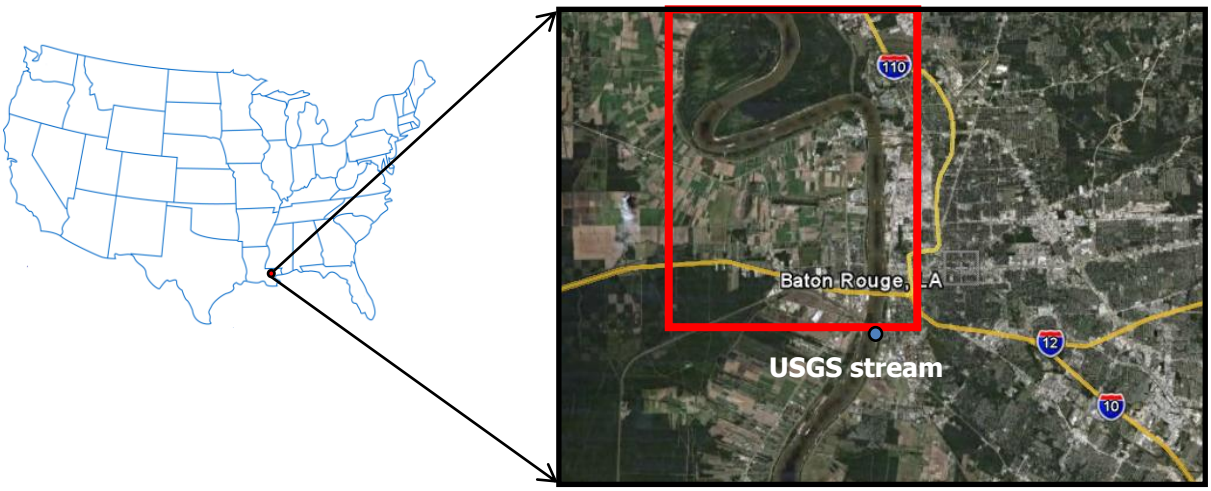

Figure 1: Location of the study section on the Mississippi River (red rectangle) including the USGS stream gauge (blue dot).

Model Grid Configuration

The shoreline for the model domain was obtained using Digital Elevation Model (DEM) data from the USGS. River-transect bathymetry data were obtained from FFP through the US Army Corps bathymetry survey library. High resolution river multi-beam bathymetries were also obtained from FFP. Both the river-transect and multi-beam bathymetry were combined and interpolated onto an orthogonal, curvilinear grid of the system to establish the bottom elevations. The model domain extends approximately 18 km

upstream of the bend to 9 km downstream. Grid cell sizes vary from 20×20 m^2 in the bend to 20×50 m^2 in the rest of the domain (23,700 cells). The vertical resolution comprises 10 sigma layers that vary in thickness depending on the bottom elevation and water depth in each cell.

MHK Array Characteristics and Flow Conditions

Three different scenarios (4-, 23-, and 112-piling arrays) were developed for SNL-EFDC simulations. Each scenario builds upon the other; the four-piling array is included within the 23-piling array and the 23-piling array is included within the 112-piling array. The 4-piling array comprises 12 turbines; the 23-piling, 124 turbines; and the 112-piling, 534 turbines. Piling locations for the three arrays are illustrated in Figure 2. Each piling consists of turbine-pair rows, as shown in Figure 3, where the number of available turbine-pairs on a piling depends on the following bottom-elevation rule:

$$\left\{\begin{array}{c} < 40 \text{ ft } = 0 \text{ turbines} \\ 40 \text{ to } 54 \text{ ft } = 1 \text{ row} - \text{pair}, 2 \text{ turbines} \\ 55 \text{ to } 69 \text{ ft } = 2 \text{ row} - \text{pair}, 4 \text{ turbines} \\ 70 \text{ to } 84 \text{ ft } = 3 \text{ row} - \text{pair}, 6 \text{ turbines} \\ 85 \text{ plus } = 4 \text{ rows} \end{array}\right\}$$

Figure 4 shows the number of turbines in each piling based on the bottom-elevation rule. The vertical spacing between the bottom of the lowest MHK turbine and the riverbed is, in general, between 3 and 7.5 m. The devices have a 1.5-m piling diameter, 3.0-m turbine diameter, and 1.5-m vertical space between the top of one turbine and the bottom of the next. The turbines are located at least 6 m below the Low Water Reference Plain (LWRP), which was specified in the Mississippi River Low Water Reference Plane (File No. H-5-55630) from the U.S. Army Engineers District, New Orleans, as equal to 1.5 m. Therefore, the topmost pair of turbines is located 6 m below the LWRP so as not to impact shipping traffic. The thrust coefficient for each MHK turbine is $C_T = 0.73$ and the piling support structure has a drag coefficient of $C_D = 1.2$. Four sets of simulations were performed corresponding to the river hydrodynamics without and with the three MHK array scenarios. The model was forced with a constant flow of 20,000 m^3/s, representing ~35% probability of exceedance flow rate (i.e. 35% of the time the flow is greater than 20,000 m^3/s for this section of the Mississippi river in a given year). This flow rate was selected as it generated velocities that exceeded 2 m/s at the turbine deployment location, providing good conditions for power generation. The outflow head was specified using the discharge/stage relationship data measured at the Baton Rouge stream gauge. The array scenarios were analyzed to study the potential hydrodynamic effects of MHK device arrays and to estimate the power generated.

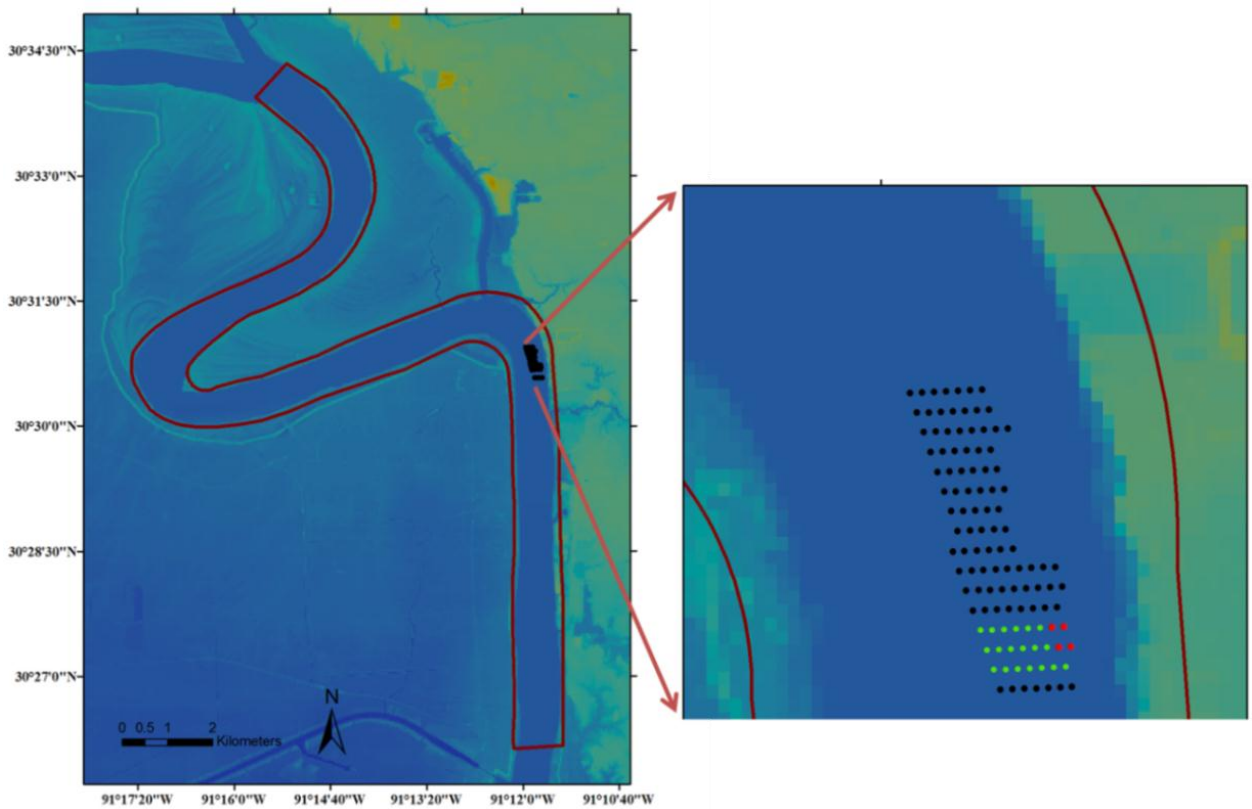

Figure 2: Location map for the arrays. The four-piling array is represented with red dots, the 23-piling array includes red and green dots, and the 112-piling arrays includes red, green, and black dots.

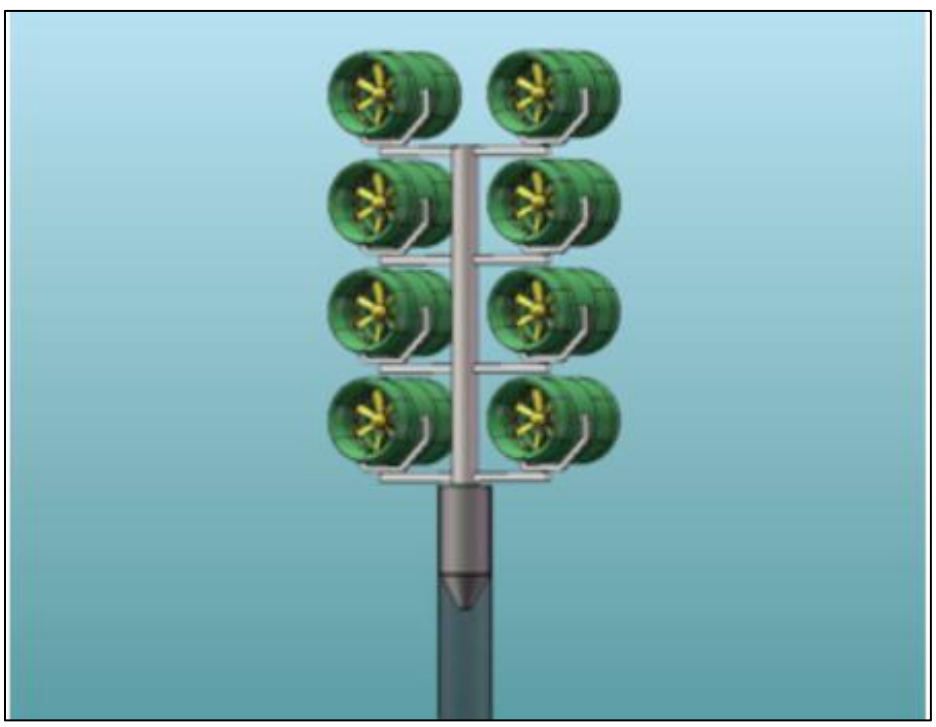

Figure 3: Concept diagram for Mississippi River FFP turbines.

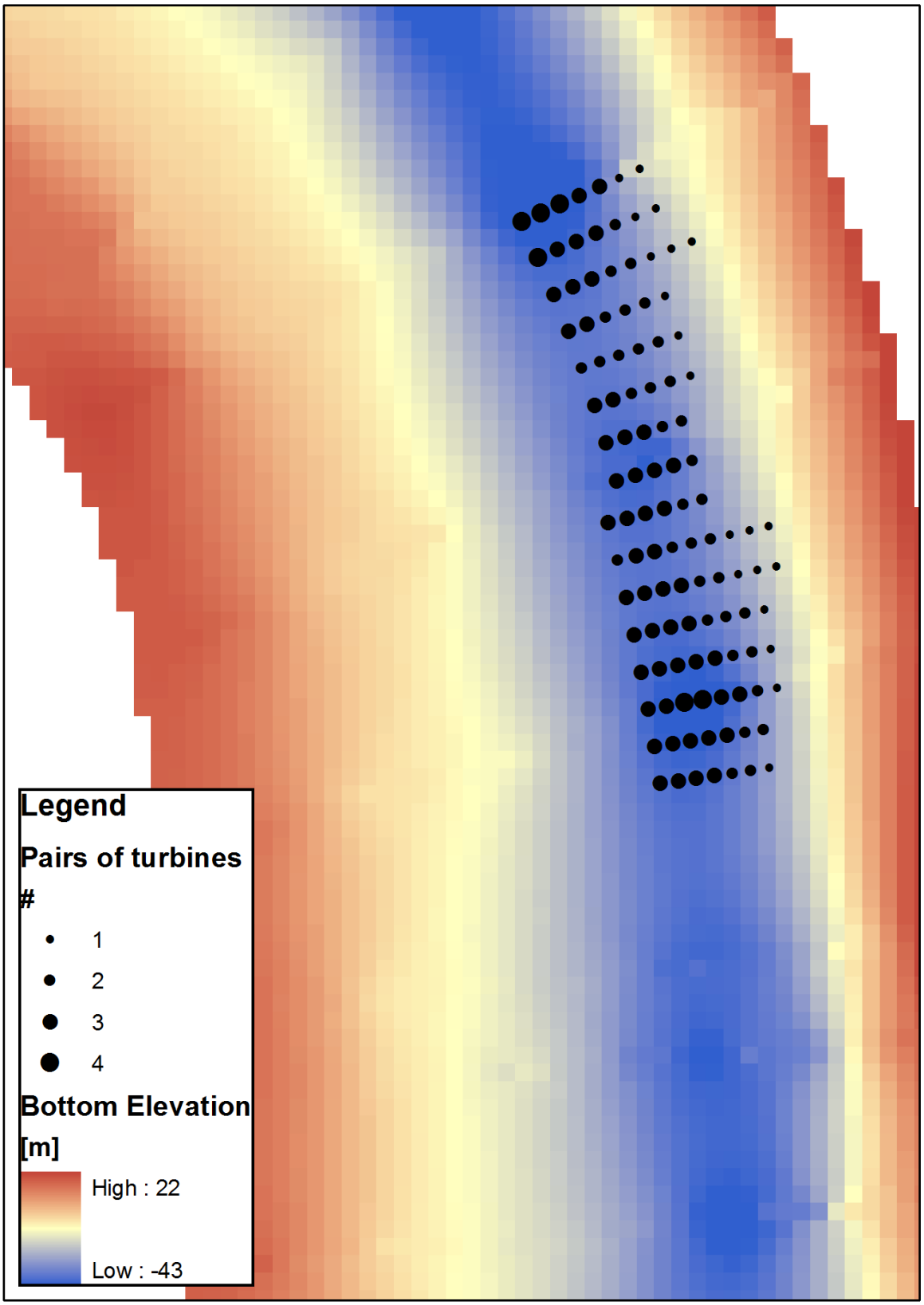

Figure 4: Number of pairs of turbines attached to each piling.

Results and Discussion

River Velocities

SNL-EFDC simulations were run for the baseline case (without MHK turbines present) and for the 4-, 23-, and 112-piling scenarios. Each model began from a restart file and the simulation was for 5 hours to ensure a steady state solution was reached. Figure 5 is the SNL-EFDC-simulated depth averaged velocity field at a flow rate of 20,000 m^3/s without an MHK array. Higher velocities are observed near the east bank of the river after the bend corresponding to the location of the MHK array (Figure 2). Depth-averaged velocities exceeding 2 m/s are observed in the faster flowing portions of the river.

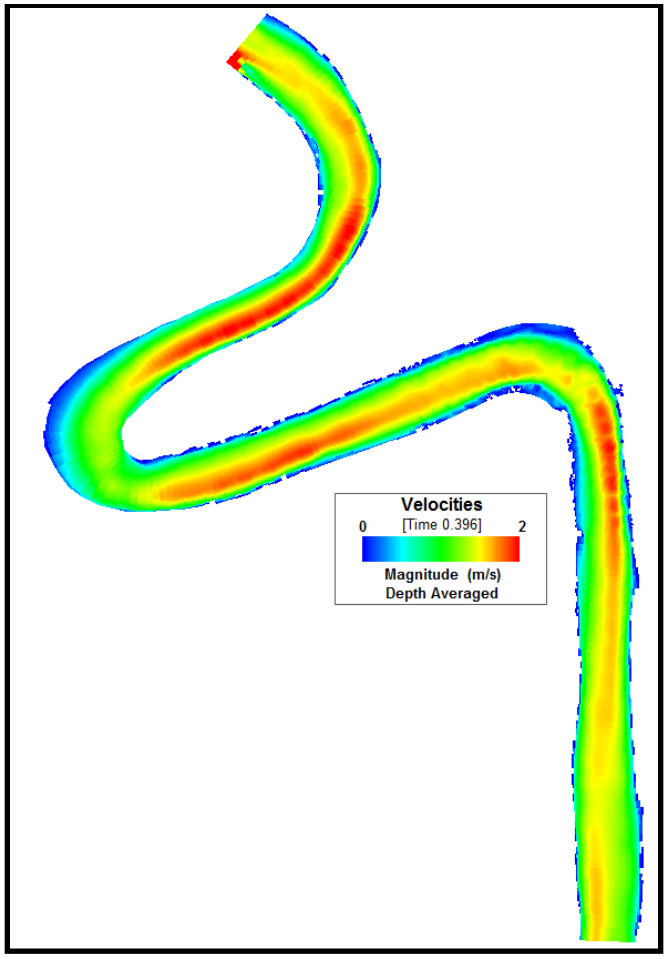

Figure 5: Simulated depth-averaged velocities without an MHK array with a constant 20,000-m^3/s flow.

For the 4-piling MHK array, Figure 6(a) shows simulated depth-averaged velocities while Figure 6(b) shows the velocities in model depth layer 4. Layer 4 was selected because a power-generating portion of every turbine-piling occupies this layer and thus showed the greatest reductions in velocities. Figure 7(a), 7(b), 8(a), and 8(b) shows the simulated depth-averaged velocities and the velocities in model layer 4 for the 23- and 112-piling MHK arrays, respectively.

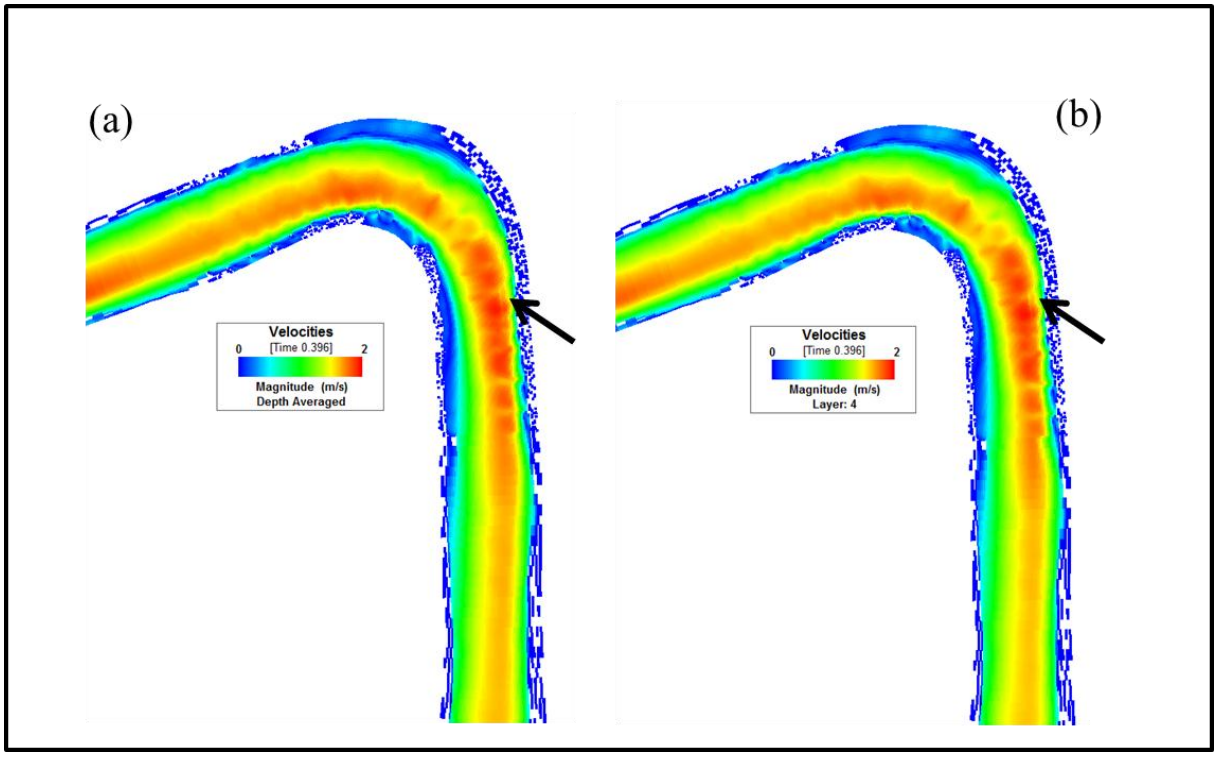

Figure 6: Simulated (a) depth-averaged and (b) layer 4 velocities with the 4-piling MHK array.

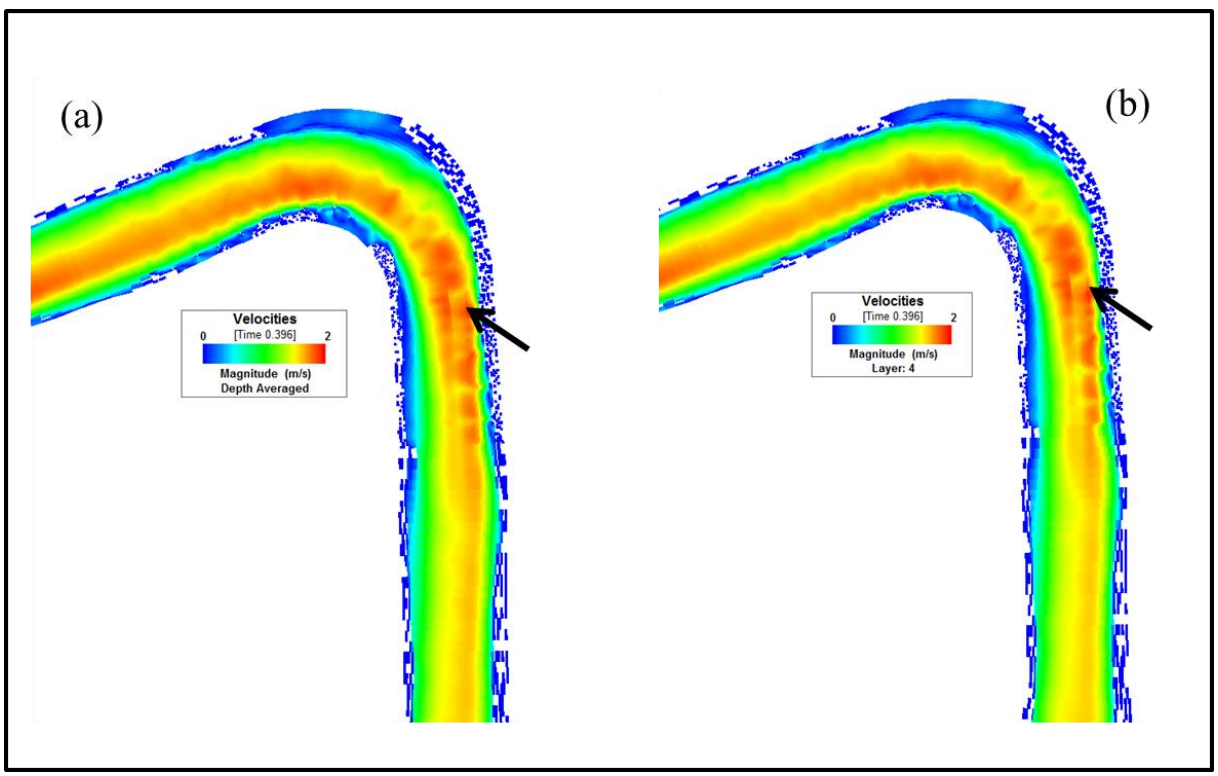

Figure 7: Simulated (a) depth-averaged and (b) layer 4 velocities with the 23-piling MHK array.

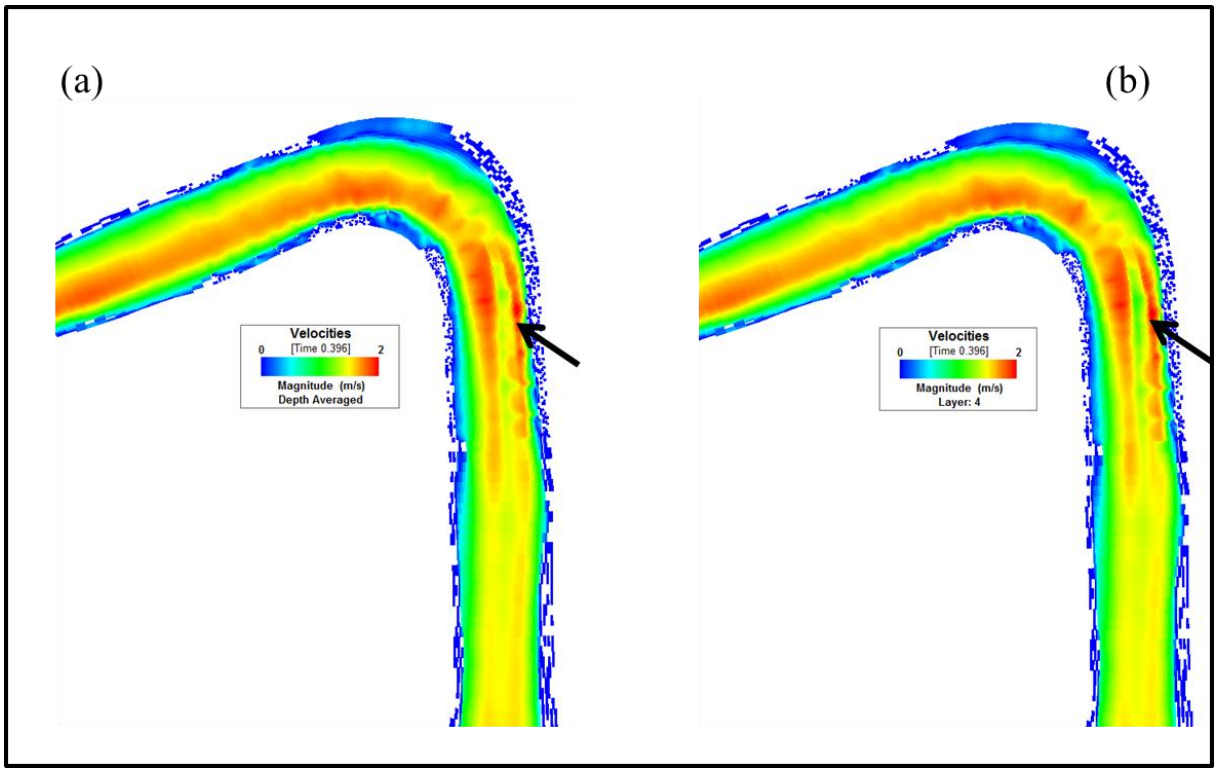

Figure 8: Simulated (a) depth-averaged and (b) layer 4 velocities with the 112-piling MHK array.

Velocity Changes

The absolute relative differences in depth-averaged velocities between the Mississippi model without and with the 4-, 23-, and 112-piling arrays are presented in Figure 9, 10, 11, and 12. Depth-averaged velocities for the three scenarios are presented using the same color-scale (from −0.3 to 0.2 m/s) for easier comparison of the hydrodynamic effects of different MHK array scenarios (see Figure 9). To illustrate the total velocity change due to each array scenario, Figure 10-12 show the absolute relative differences in depth-averaged velocities for each array with a unique color scale. Maximum velocity deficits correspond to the locations of the MHK devices. The 4-piling (12-turbine) array shows minimal velocities differences (up to 10 cm/s), while 112-piling (534-turbine) array has velocity differences up to 80 cm/s. The velocity deficit "wake" persists for about 15 array widths downstream (n.b. array width is measured in the cross-stream direction and is about 180 m). This mirrors the approximate recovery of the wake for a single MHK turbine in a straight channel, which exhibits a 10% deficit around 15 device diameters [*Bahaj et al.*, 2007; *James et al.*, 2012; *Myers and Bahaj*, 2009; 2010; *Myers et al.*, 2011]. Depth-averaged velocities and velocity profiles show decreasing velocities through and behind the MHK array as energy is generated, turbulence introduced, and flow obstructed. Recovery of the flow velocity is observed within about 20 array widths downstream of each MHK array.

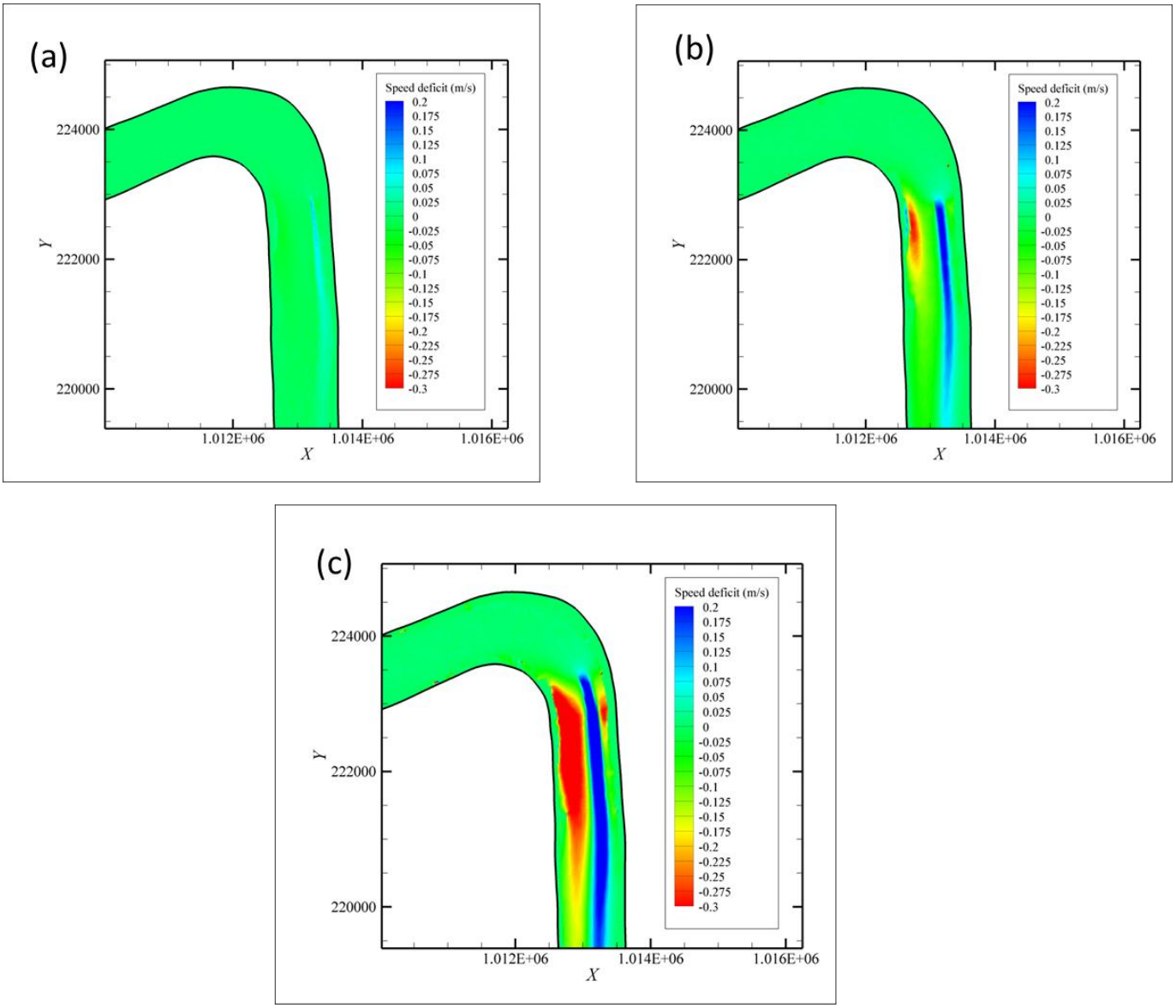

Figure 9: Absolute relative differences in depth-averaged velocities between the Mississippi model without and with the (a) 4-, (b) 23-, and (c) 112-piling arrays. Note that the same color scale is used in each figure.

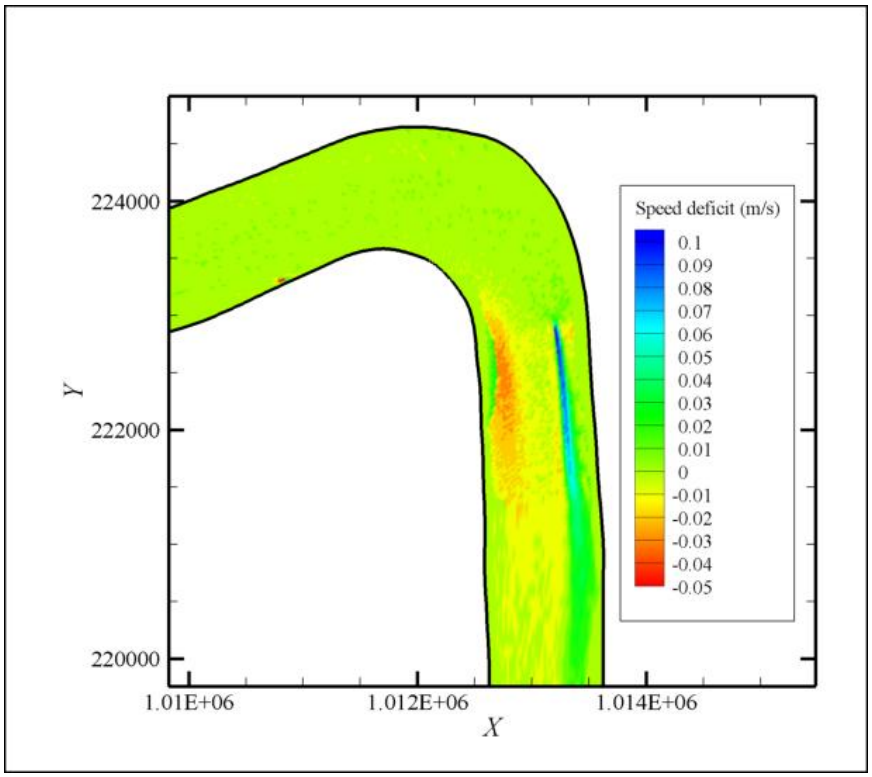

Figure 10: Relative differences in velocities between simulations without and with the 4-piling MHK array.

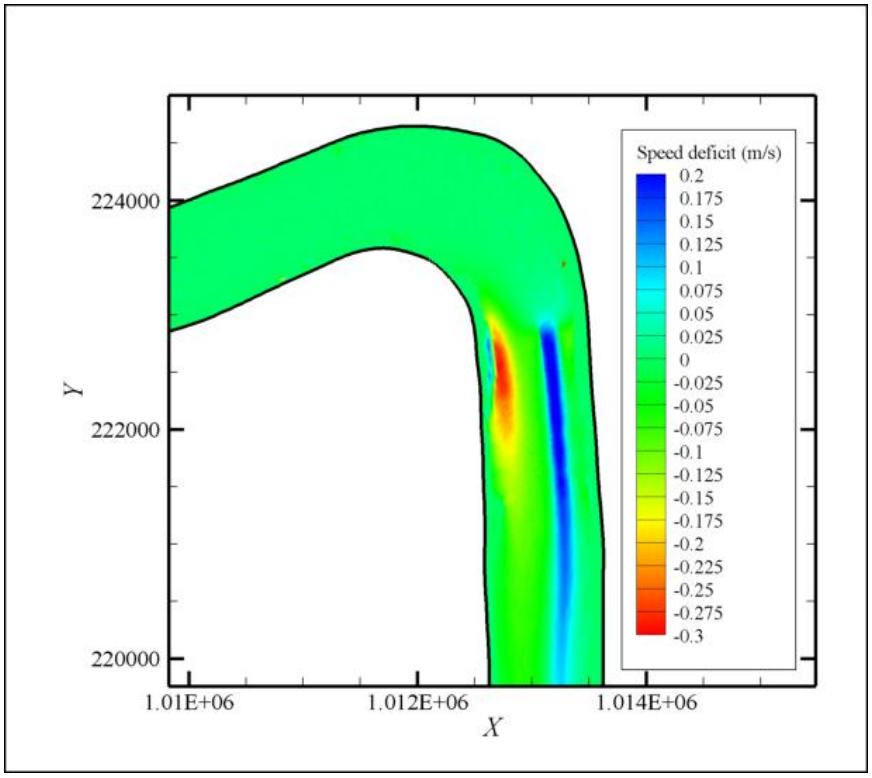

Figure 11: Relative differences in velocities between simulations without and with the 23-piling MHK array.

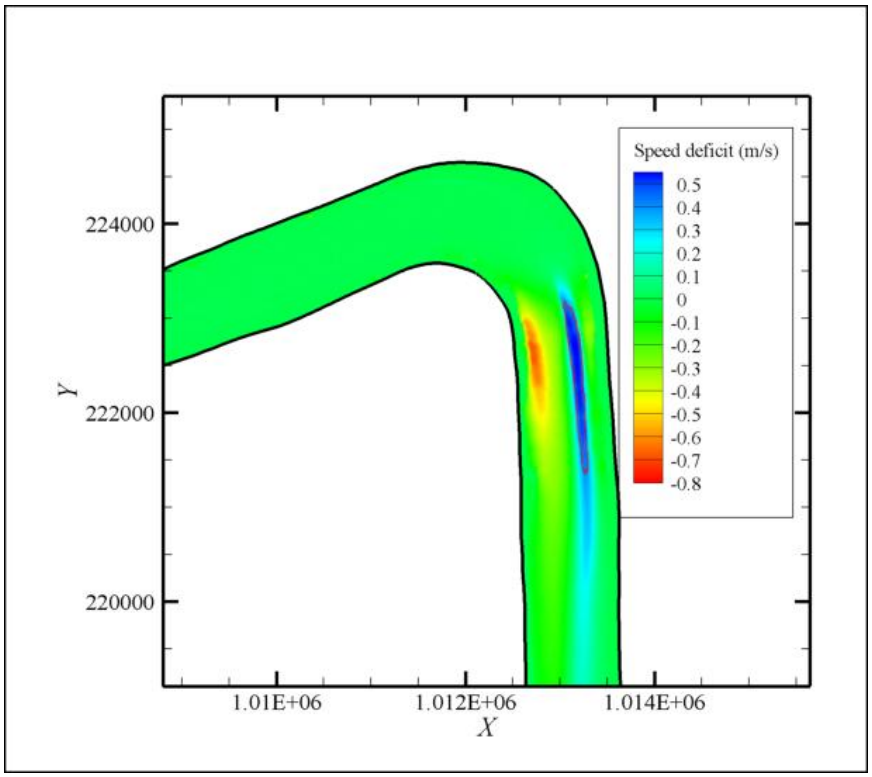

Figure 12: Relative differences in velocities between simulations without and with the 112-piling MHK array.

Water-Level Changes

Differences in water elevation without and with the (a) 4-, (b) 23-, and (c) 112-piling arrays using the same color-scale are presented in Figure 13. Differences in water elevation with unique color scales are presented in Figure 14-16. Water depth increases upstream of the MHK devices by up to 2 mm in the 4-piling array, 1.6 cm in the 23-piling array, and 5.5 cm in the 112-piling array due to flow obstruction. Although these changes are only a small fraction of the river depth, it should be noted that they are likely an environmentally conservative estimate. This is due to the combination of the pressure-head boundary condition on the south (outflow) boundary and the finite size of the domain; all depth increases must occur upstream of the array. In reality, the situation is more complicated and the water level is likely to be more evenly distributed upstream and downstream yielding a smaller maximum depth increase. The depth increase in the vicinity of the array is a result of the turbines converting pressure head to energy. As the flow reorganizes and the wake dissipates, the water depth recovers and becomes uniform across the river.

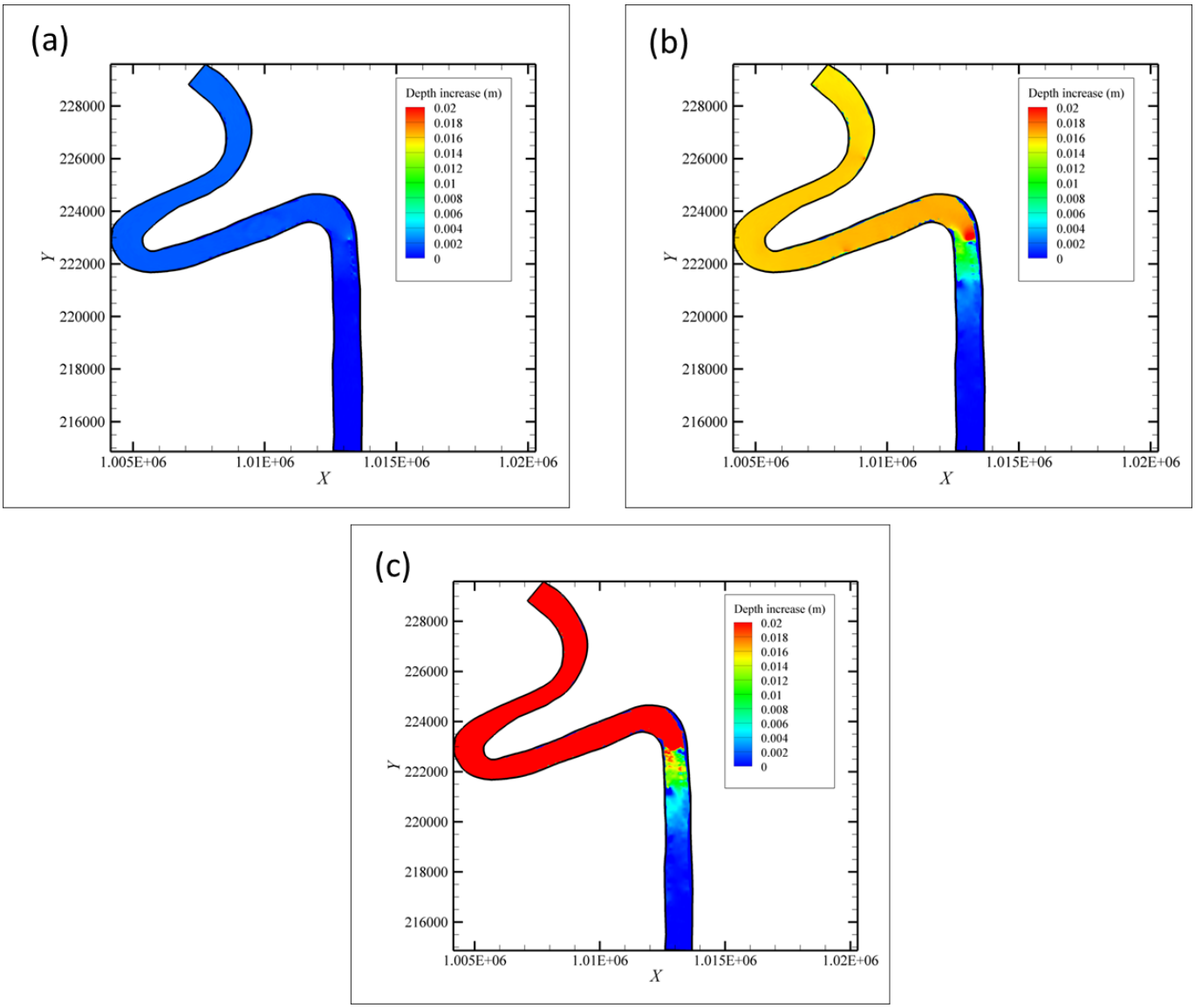

Figure 13: Differences in water elevation without and with the (a) 4-, (b) 23-, and (c) 112-piling arrays. Note that the same color scale is used.

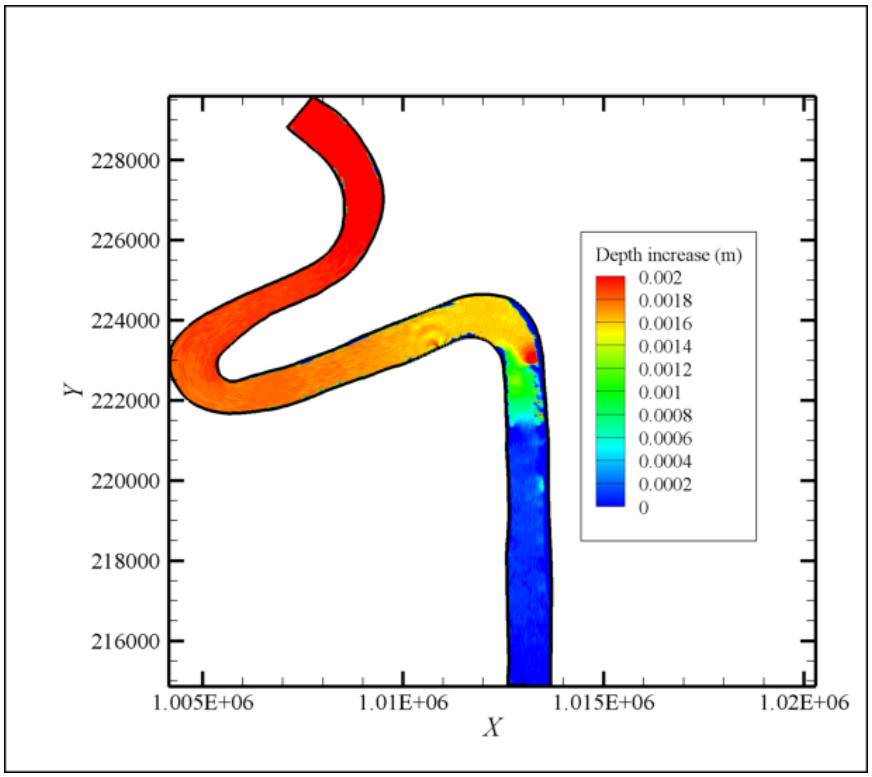

Figure 14: Differences in water elevation without and with the 4-piling MHK array.

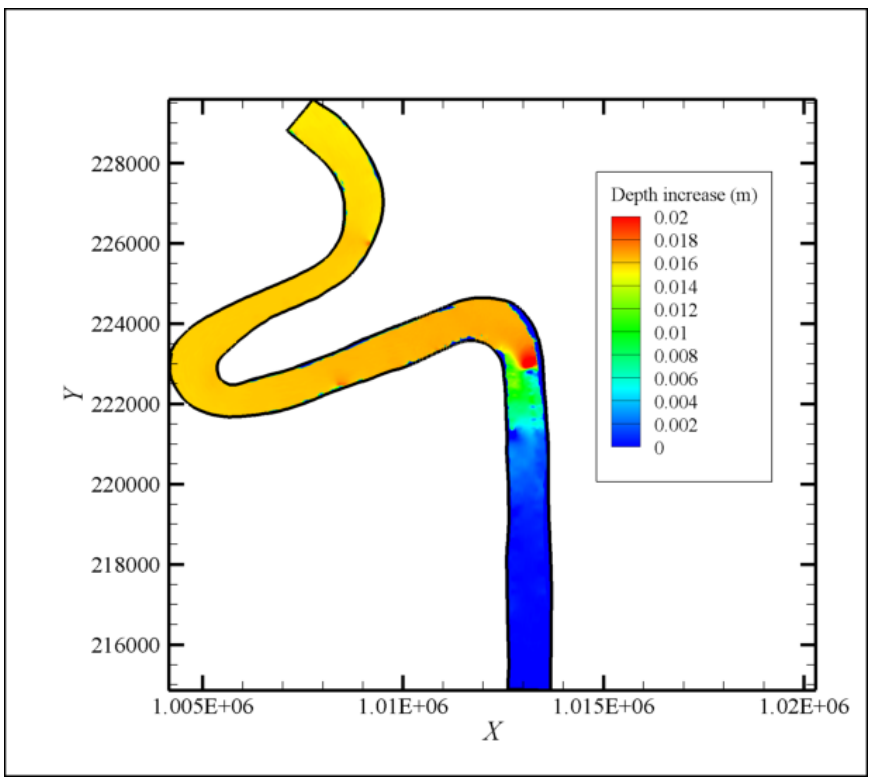

Figure 15: Differences in water elevation without and with the 23-piling MHK array.

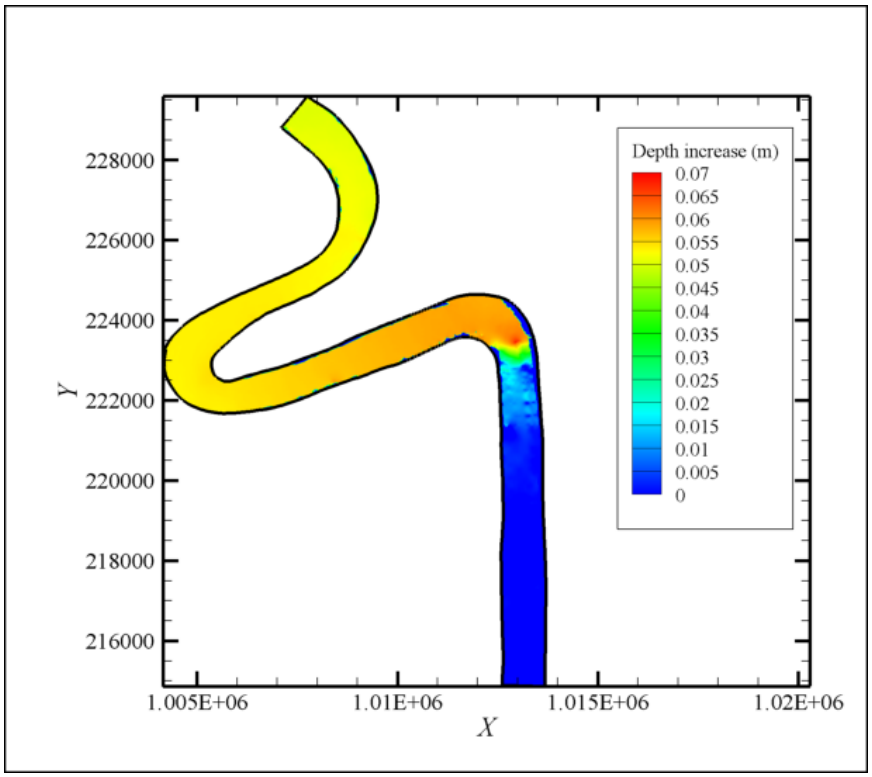

Figure 16: Differences in water elevation without and with the 112-piling MHK array.

Power Generation

The estimated total power generated in the three arrays is listed in Table 1. This project marks the first time that SNL has been requested to predict power from multiple turbines mounted vertically on a single structure (the Free Flow Power design). As a first pass, power generation estimates are based on the flow facing area of the overall footprint of all of the turbines on a given pile. The actual turbine swept area is necessarily smaller than the turbine/piling footprint area and therefore these power generation estimates will be slightly over predicted. The difference between the actual turbine swept area and the total turbine footprint for a given pile is dependent on the number of turbine pairs because each turbine pair is separated by a ½ a turbine diameter in the vertical; therefore the power generation estimates become slightly more over predicted as the number of turbine pairs increases (and hence the difference in flow facing areas slightly increases). This discrepancy as well as other sources of uncertainty in predicting turbine power output will be further investigated to increase the accuracy of power prediction estimates moving forward.

Table 1: Total power generated by each array and average turbine output.

Array	Total energy generated by the array [MW-hr]	Energy generated in the array per turbine [MW-hr]
4-piling MHK	0.20	0.0167
23-piling MHK	2.49	0.0201
112-piling MHK	7.65	0.0143

An estimate of the average power contribution for the turbines on a given pile for the 112-piling MHK array was calculated by dividing the power generated by each piling by the corresponding number of turbines on a specified pile (Figure 17). The depth averaged velocity for the location of each piling is presented in Figure 18. As observed in the average power contribution of each piles turbines (Figure 17), turbine power is primarily dictated by the flow velocities. It is also observed that the piling power contribution depends not only on the flow velocities, but also on the corresponding number of turbine pairs in the piling (see Figure 4). In summary, the power contribution of each piling is primarily dictated by the flow velocities, number of pairs of turbines, and bathymetry.

Additionally, another estimate of efficiency is the average performance of all the turbines in the array (array performance). As can be seen in Table 1 the 23-piling array generates more energy per turbine than either the 4 or 112-piling arrays. This is counter to analyses done in constant depth rectangular flumes [*Johnson et al.*, 2011] that demonstrate a regular reduction in efficiency as the number of turbines is increased over a given footprint. The deviation is a result of the intricate balance between natural river flow around the bend, variable water depths and the increased footprint of the deployment area. The 112-piling commercial array is the least efficient array configuration but generates significant power. As mentioned previously, these preliminary array configurations were developed by Free Flow Power and a great starting point to springboard further investigations of array optimization to maximize power production and minimize environmental effects.

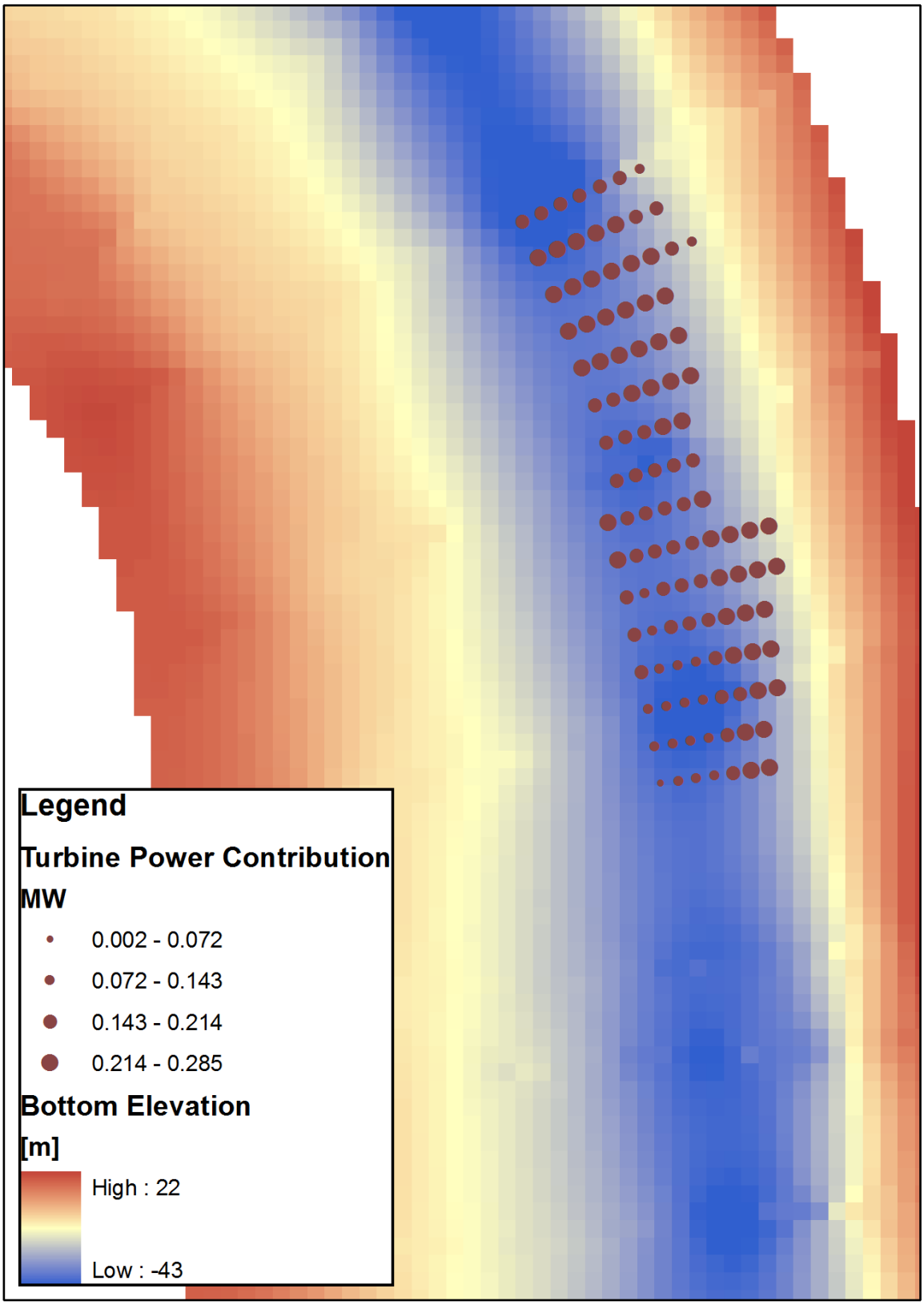

Figure 17: Average turbine power contribution for each of the 112-pilings in the MHK array.

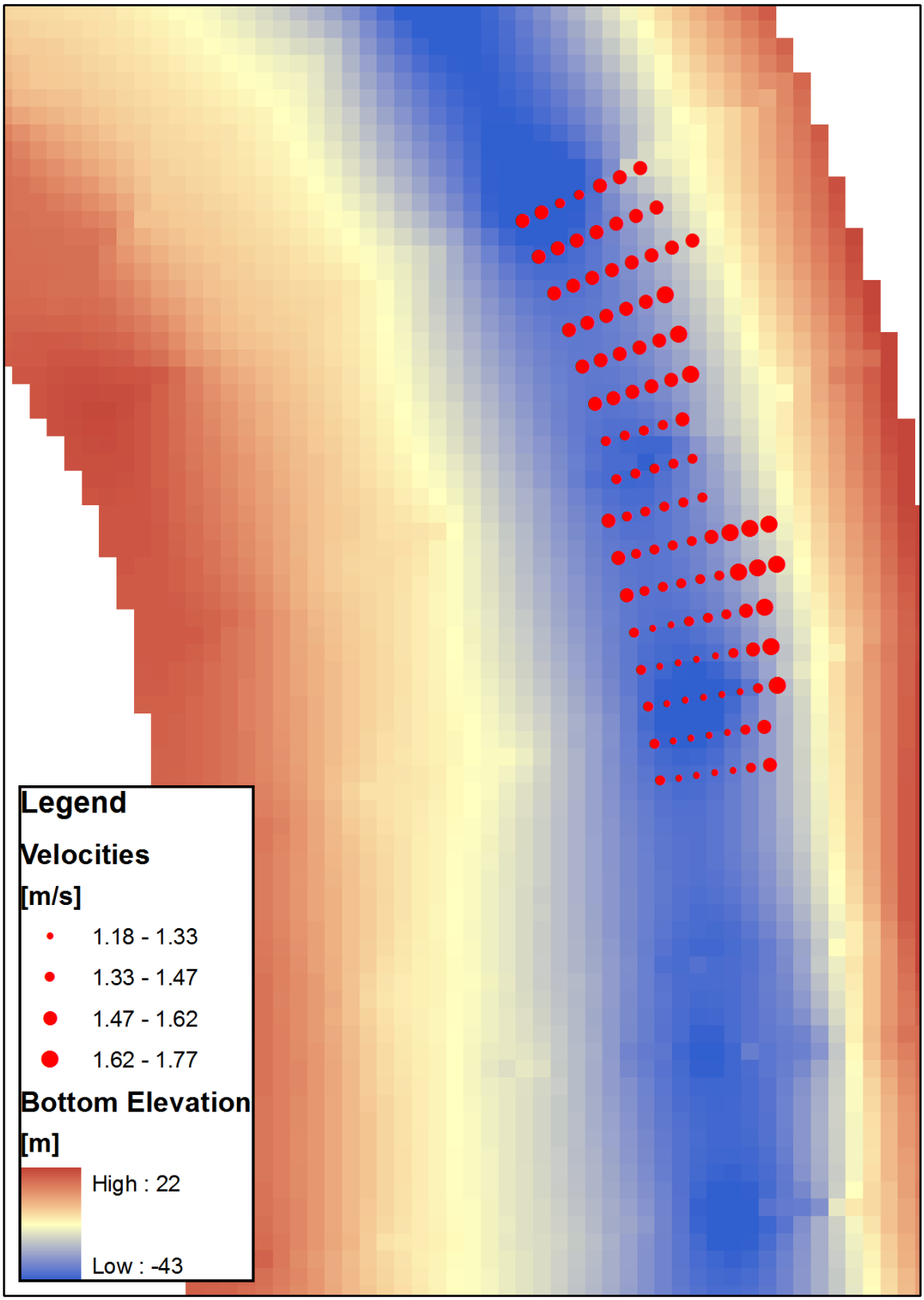

Figure 18: Depth averaged flow velocity in the location of each piling for 112-piling MHK array.

Sediment Dynamics

Sandia has expended considerable R&D efforts to upgrade EFDC to include state-of-the-art sediment dynamics simulation capabilities. Specifically, the SEDLZJ [*Jones*, 2001; *Jones and Lick*, 2001] algorithms were incorporated into SNL-EFDC. The new approach in SNL-EFDC is an extension of previous models and accounts for multiple sediment size classes, has a unified treatment of suspended load and bedload, and appropriately replicates bed armoring. The resulting flow, transport, and sediment dynamics model is an improvement to previous models because it may directly incorporate site-specific data, while maintaining a physically consistent, unified treatment of bedload and suspended load [*James et al.*, 2010].

As a proof of concept of SNL-EFDCs ability to simulate sediment dynamics, a simplified sediment erosion model was developed. In this model, the uniform sediment bed was defined to comprise three sediment size classes, with one-third mass fractions of sizes 1,020, 5,000, and 10,000 μm. While these are unrealistically large sediment size classes for the Mississippi River at this location, they were selected because the high shear-stress environment of a 20,000-m^3/s flow tends to erode sediment quite quickly. While the real system is probably composed of course sand over hard-pan mud , without specific sediment size and erosion information data collected from the site, these size classes are reasonable surrogates for a sediment bed that is fairly resistant to erosion. The sediment bed was defined as 51 cm deep with an un-erodible layer on the bottom. This simplistic definition allows an analysis of where the sediment bed is likely to erode (or aggrade) depending on the local flow characteristics, which are certainly impacted (as noted above) by operation of an MHK array.

Shear Stress

To simulate sediment dynamics, it is important to have an accurate estimate of bed shear stress because erosion rates may vary as shear stress raised to a power of order 2-3 (Roberts et al. 1998). Shear stresses without an MHK array and changes in shear stress for the three arrays are presented in Figure 19 and 20, respectively. Shear stress is proportional to the square of the velocity, so high shear areas correspond to high-velocity areas. Decreases in shear stress are observed behind the MHK arrays. These are regions where sediment might accumulate (or at least where erosion would be decreased).

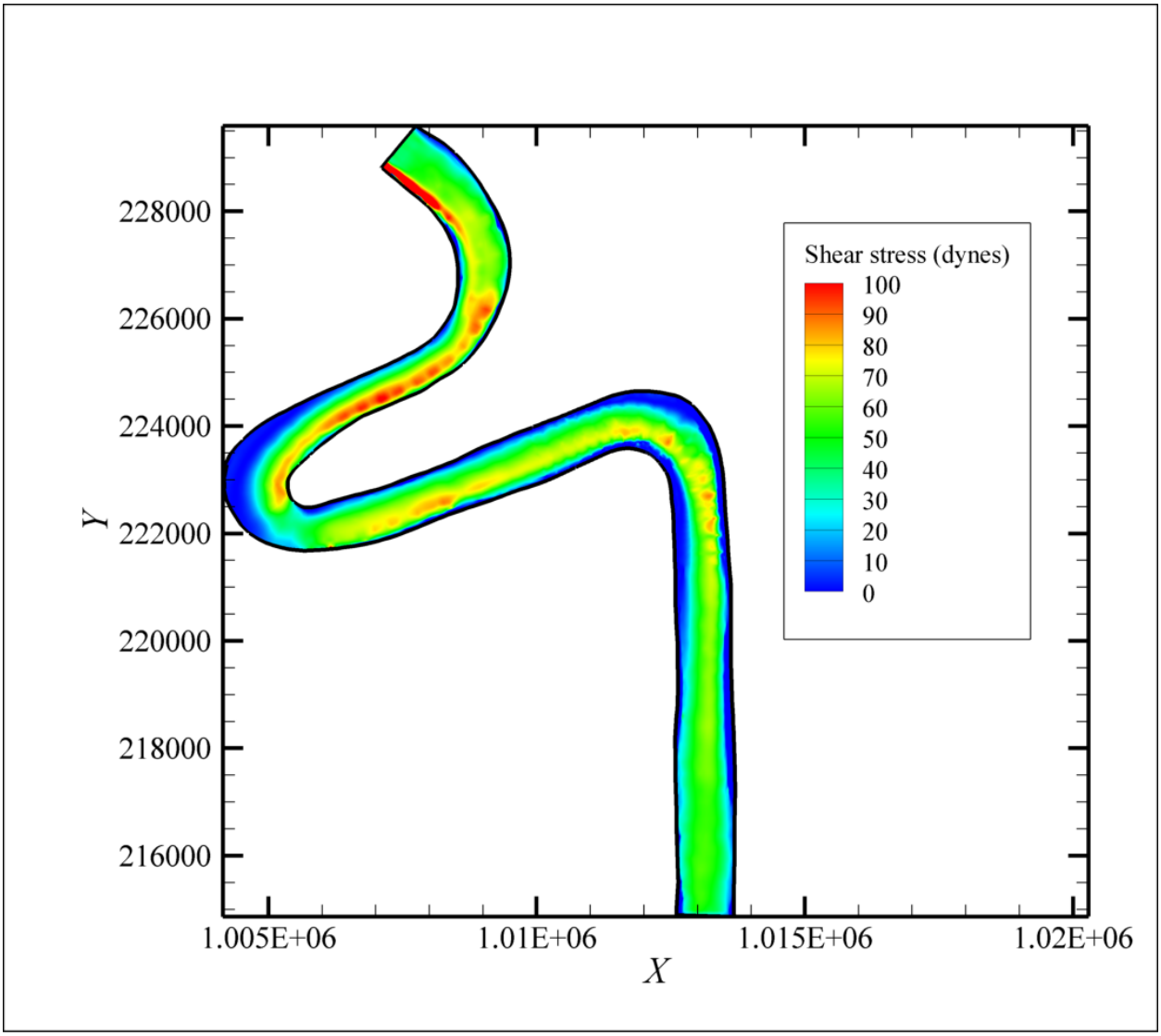

Figure 19: Simulated shear stress without an MHK array due to a constant 20,000-m^3/s flow.

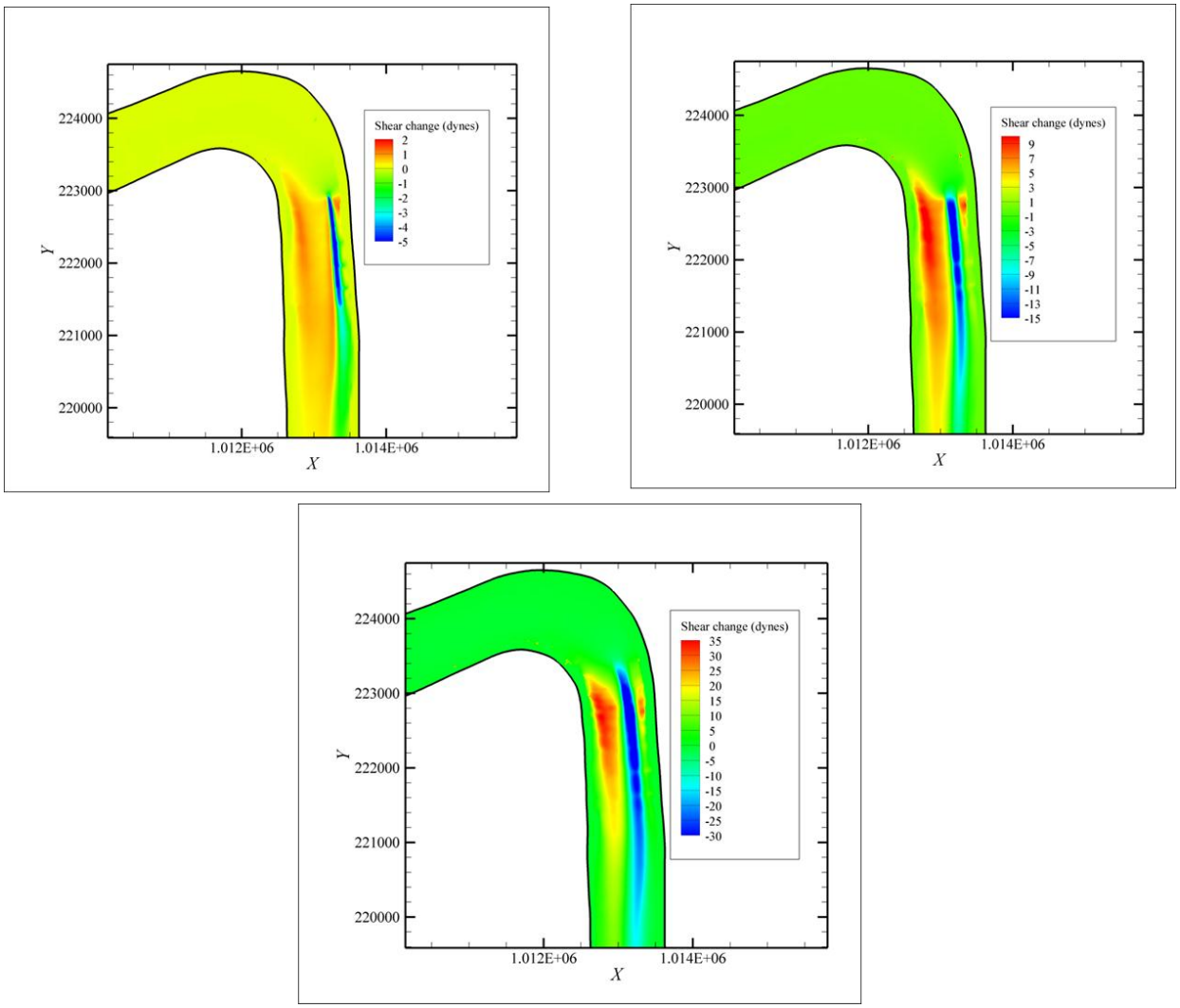

Figure 20: Shear stress changes with (a) 4-, (b) 23-, and (c) 112-piling arrays.

Erosion

Change in sediment bed thickness after 5 hours of erosion (where the bed started 51 cm thick) without MHK and for the 112-piling MHK array are presented in Figure 21 and 22. Although this is a contrived case, it demonstrates the utility of SNL-EFDC in assessing changes to sediment dynamics due to MHK array operation. As expected, the simulations both without and with turbines show decreases in bed thickness corresponding to regions of high flow velocity and shear stress. In fact, at the high shear stresses of this 20,000-m^3/s flow and for this contrived sediment bed, the entire bed is eroded in many locations. Downstream of the 112-piling MHK array, however, the model shows decreased erosion (thicker sediment bed) due to the decreased flow velocities in the wake of the MHK devices. Also, there is some increase erosion (evident as a decreased sediment bed thickness) around the sides of the array where flow is diverted due to flow obstruction.

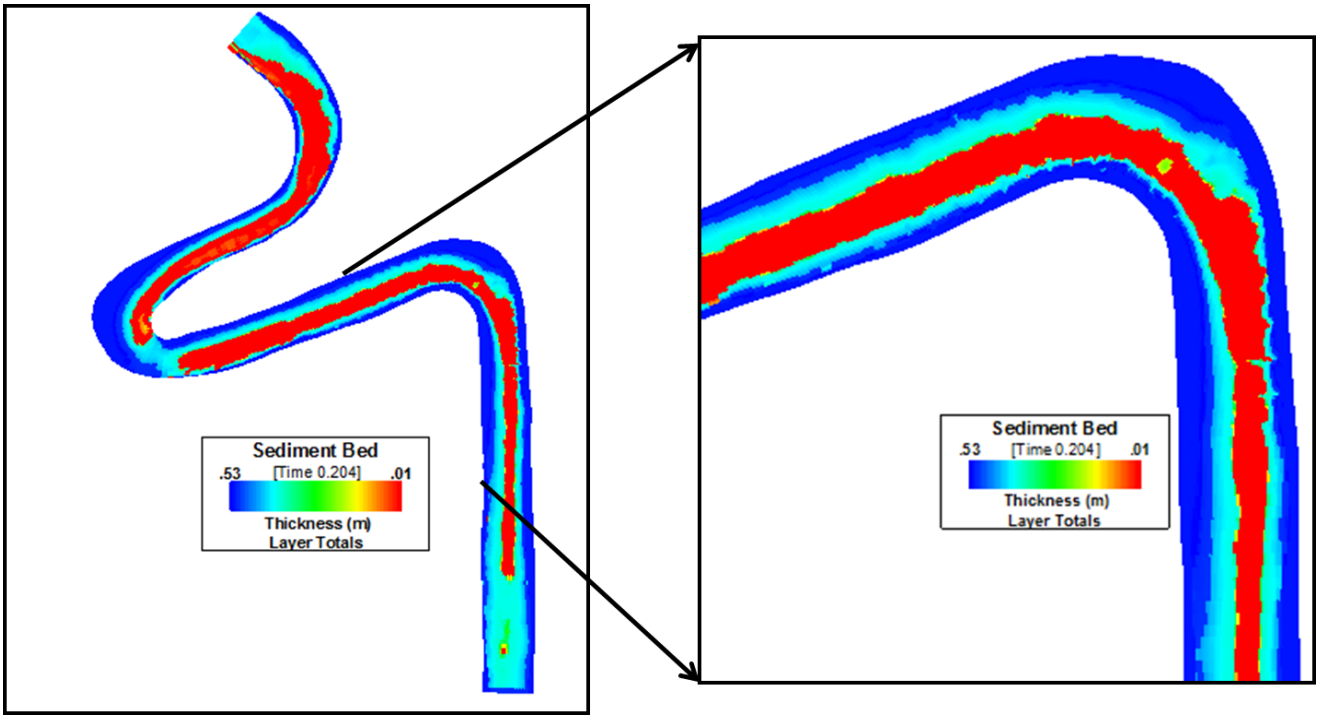

Figure 21: SNL-EFDC example erosion estimates without MHK arrays for the whole domain (left) and a close up where the turbines would be placed (right).

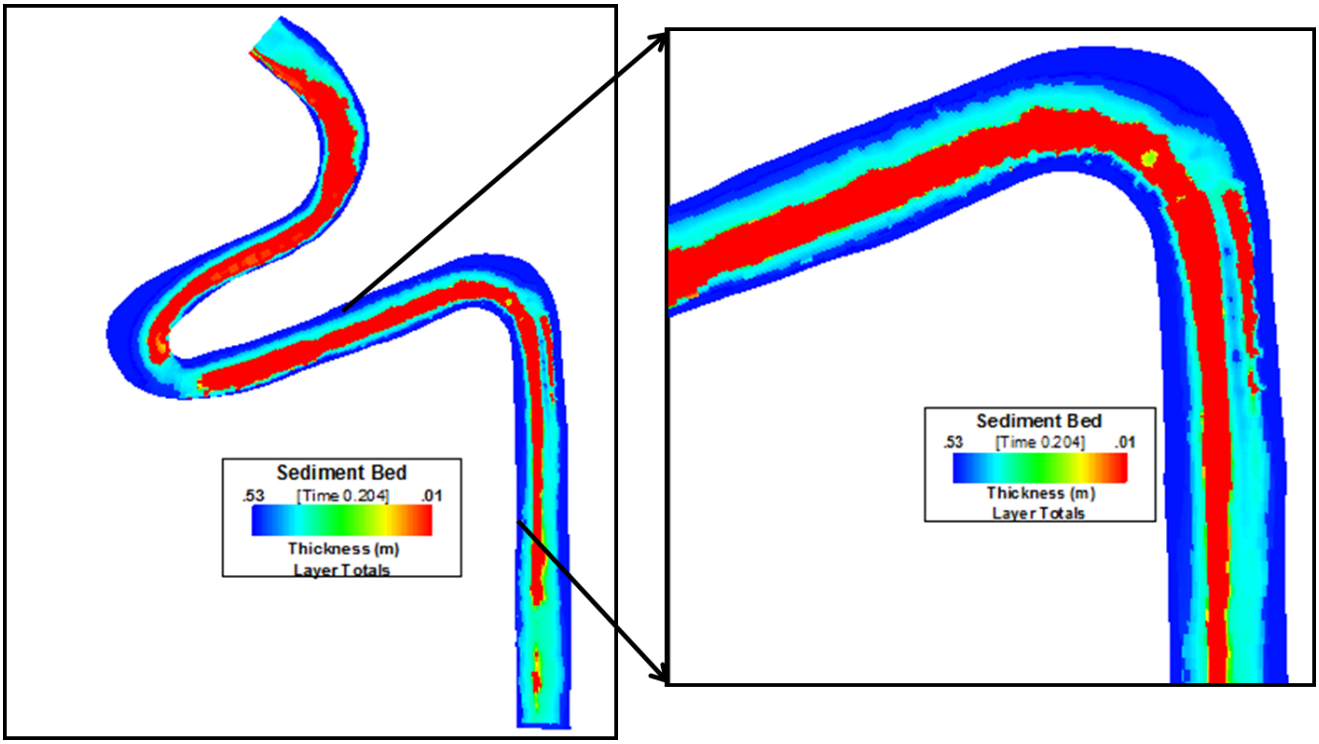

Figure 22: SNL-EFDC erosion estimate for the 112-piling MHK array for the whole domain (left) and a close up where the turbines are placed (right).

Summary and Discussion

The output of this preliminary modeling effort can help provide early guidance on optimal array configuration and also help specify control methods to determine the effects of arrays on site hydrodynamics, sediment transport, and water quality. Flooding in the Mississippi River is a primary concern for regulators and managers of river operations. Therefore, SNL has targeted water-level evaluation in this first analysis. Initial results indicate that the deployment of 12 turbines in 4 piling, 124 turbines on 23 pilings, and 534 turbines in 112 piling does not present a significant flooding hazard (ranging from maximum water elevation gains resulting from this turbine configuration between 2 and 5 cm for river flows of 20,000 m^3/s). As the flow increases, there is a complex interplay of water depth, depth-averaged velocities, and power generation; both depth and velocity increase nonlinearly while power generation increases as the square of the flow rate. Changes to relative velocity are non-monotonic and require modeling to identify patterns. This is because all three variables (depth, flow rate, and power generated) change simultaneously. Overall, this is an encouraging result that should support FFP deployment efforts (i.e., estimated increases to upstream depth are only a small fraction of the flow depth on the order of less than a tenth of a percent). Future efforts may include running flood-like flow scenarios to ensure that flooding hazards are not elevated under the highest of flow rates.

For these three array scenarios, more overall power was produced as the numbers of turbines increased. However, individual turbine power efficiency was greatest for the scenario 2 configuration. This provides a glimpse into the complexity of flow in natural systems with variable water depths, bends, and introduction of flow disturbances (i.e. turbines and their foundations). A proof of concept sediment transport model was built and applied to demonstrate the general changes expected in sediment dynamics as a result of the operation of MHK-turbines. In general, the flow was increased around the turbines as a result of the flow diversion creating higher shear at the sediment bed and opportunity for increased erosion locally. Downstream of the MHK array, however, the decreased flow in the wake caused erosion potential to decrease which could actually cause sediments to deposit and accumulate over time. More detailed hydrodynamic and sediment transport studies will be the focus of efforts in FY13.

References

Bahaj, A.-B. S., L. E. Myers, M. D. Thomson, and N. Jorge (2007), Characterising the wake of a horizontal axis marine turbine, in *7th European Wave and Tidal Energy Conference*, edited, pp. 1-9, Porto, Portugal.

James, S. C., C. A. Jones, M. D. Grace, and J. D. Roberts (2010), Advances in sediment transport modelling, *Journal of Hydraulic Research*, *48*(6), 754-763.

James, S. C., E. Johnson, J. Barco, J. D. Roberts, and C. A. Jones (2012), Simulating flow changes due to marine hydrokinetic energy devices: SNL-EFDC model validation, *Renewable Energy*, *submitted*.

Johnson, E., J. Barco, S. C. James, and J. Roberts (2011), Reference model MHK turbine array optimization study within a generic river system, *Sandia Report*, *SAND2011-9305*.

Jones, C. A. (2001), A Sediment Transport Model, PhD thesis thesis, 119 pp, University of California Santa Barbara, Santa Barbara.

Jones, C. A., and W. Lick (2001), Sediment erosion rates: Their measurement and use in modeling, in *Texas A&M Dredging Seminar*, edited, pp. 1-15, ASCE, College Station, Texas.

Myers, L. E., and A. S. Bahaj (2009), Near wake properties of horizontal axis marine current turbines, in *Proceedings of the 8th European Wave and Tidal Energy Conference*, edited, pp. 558-565, Uppsala, Sweden.

Myers, L. E., and A. S. Bahaj (2010), Experimental analysis of the flow field around horizontal axis tidal turbines by use of scale mesh disk rotor simulators, *Ocean Engineering*, *37*, 218-227.

Myers, L. E., B. Keogh, and A. S. Bahaj (2011), Experimental investigation of inter-array wake properties in early tidal turbine arrays, paper presented at OCEANS 2011, 19-22 Sept. 2011.